Key Engineering Materials
ISSN: 1662-9795, Vol. 926, pp 46-55

Submitted: 2021-11-30
Accepted: 2022-01-24
Online: 2022-07-22

A Comprehensive Analysis of AISI 316L Samples Printed via FDM: Structural and Mechanical Characterization

M. Carminati[1,a,*], M. Quarto[1,b], G. D'Urso[1,c], C. Giardini[1,d], C. Borriello[2,e]

[1]Department of Management, Information and Production Engineering – University of Bergamo, Via Pasubio 7/b, 24044, Dalmine (BG), Italy

[2]SSPT-PROMAS-NANO - CR ENEA Portici, p.le E. Fermi 1, 80055, Portici (NA), Italy

[a]mattia.carminati@unibg.it, [b]mariangela.quarto@unibg.it, [c]gianluca.d-urso@unibg.it, [d]claudio.giardini@unibg.it, [e]carmela.borriello@enea.it

Keywords: AISI 316L, Metal FDM, density evaluation, porosity, mechanical properties, XRD

Abstract. Metal Fused Deposition Modelling is a promising multi-step process able to manufacture metal parts by means of a low-cost additive technique. In this study, a metal-polymer composite filament characterized by homogenous mixture of AISI 316L sinterable metal powders and a multi-component polymeric matrix was used to fabricate samples by means of a FDM printer. A 2^4 full factorial design of experiments was elaborated to define the possible influence of the relevant printing parameters on dimensional shrinkage, bulk density and overall porosity of printed samples. In addition, the mechanical properties of printed AISI 316L samples were investigated by performing tensile tests, compression tests, Charpy impact tests, Rockwell B and Vickers hardness tests. An X-ray diffraction analysis was conducted to assess the crystallographic structure of the FDM AISI 316L samples.

Introduction

The term Additive Manufacturing (AM) was introduced in the 1990s to describe a new technology capable of manufacturing 3D components by joining materials, usually layer upon layer, as alternative to subtractive and formative manufacturing technologies [1].

Fused Deposition Modelling (FDM) is one of the most widely used AM technologies owing to its simplicity and low costs. In the FDM process, extruded materials are generally thermoplastic filaments with poor mechanical properties. Additionally, highly-filled polymer filaments for the Additive Manufacturing of metal parts exist to enhance multiple properties of polymer composites. A few studies have been conducted on the reinforcement of polymeric filaments. Hwang et al. [2] stated that the tensile strength of specimens decreases by raising the copper contents. Likewise, Ryders et al. [3] confirmed the deterioration of the mechanical properties of samples with the addition of type 420 stainless steel particles. Indeed, polymer-metal composites reduce the mechanical performances due to difficulties in achieving uniform particle distribution and strong adhesion between metal powders and polymer matrix generating large voids.

Shaping, debinding and sintering [4] is a promising multi-step FDM variant, that overcomes the limits associated with the poor mechanical properties of highly-filled polymeric filaments. The shaping phase is performed with filaments characterized by a homogenous mixture of sinterable metal powders and a multi-component binder system. A debinding process is necessary to remove the polymeric fraction from the printed part; afterwards, the sintering process provides a near full densification of the metallic particles [5].

To date, in literature, only few studies are focused on mechanical properties of metal parts fabricated via FDM. Liu et al. [6] reported that the average tensile strength of 316L stainless steel parts printed by FDM was 441 ± 27 MPa and the micro Vickers hardness on average was approximately 145 ± 6.7 HV. A similar value of tensile strength was measured in [7]. Differently, Gong et al. [8] analyzed the mechanical properties of samples fabricated using two different AM techniques. The results of these tests indicated that AISI 316L samples printed by FDM process have lower yield strength, UTS, and elastic modulus compared to AISI 316L specimens printed by

Selective Laser Melting. Based on these considerations, this topic can be considered still under debate.

The present paper aims to assess the technical feasibility of an additive manufacturing process based on FDM technology combined to an innovative multicomponent binder filament loaded with 316L austenitic stainless steel. After shaping, the 3D printed components are treated by debinding and sintering processes to achieve full metallic samples.

The impact of the main FDM process parameters on the physical, mechanical and dimensional properties of the produced parts was analyzed and the samples characteristics were compared with monolithic AISI 316L properties.

Methodology

Equipment and material

The testing samples were performed using an Ultimaker 5S 3D printer. It was equipped with a direct driver extruder with a hardened steel nozzle having a diameter equal to 0.6 mm. A multicomponent binder filament (BASF Ultrafuse 316L) loaded with 316L austenitic stainless steel powder (90% wt) with a diameter of 2.85 mm was used.

After the printing phase, the samples undergo a catalytic debinding process, in which the primary binder is removed. The subsequent sintering process at temperatures slightly below the melting point of the metal allows to remove the backbone (secondary binder) and to sinter the metal particles, providing a near full densification of the metal parts.

Plan of experiments

Prismatic samples were printed for the structural analysis. The experimental campaign was based on a general 2^4 full factorial design featured by 4 factors on 2 levels (low and high): nozzle temperature (T_{nozzle}), infill pattern (In), print speed (s) and layer thickness (h). The selected printing parameters are reported in Table 1. Four repetitions were considered for each combination of the process parameters.

Table 1. 2^4 factorial design.

Parameters		Low level	High level
Nozzle temperature [°C]	T_{nozzle}	170	240
Infill pattern	In	Line 	Wall 
Print speed [mm/s]	s	20	50
Layer thickness [mm]	h	0.1	0.4

Shrinkage and density measurement

The printed samples were measured by a coordinate measuring machine (CMM) obtaining values along XY plan and Z directions. The measurements were performed for both green-parts and samples after debinding and sintering to calculate the dimensions and the volume of samples before and after the thermal treatments. The measurements were repeated three times to ensure the accuracy of the procedure and the average values were used as reference data for the analysis. The dimensional shrinkages were calculated as the percentage reduction along the three directions, according to Eq. 1:

$$\text{Shrinkage}_i = \frac{D_{gpi} - D_{ppi}}{D_{gpi}} \cdot 100. \quad (1)$$

where i indicates the dimensions (XY or Z), D_{gp} and D_{pp} indicate the dimensions of the green part and the post processing part respectively.

The density (ρ_{bulk}) of the samples was calculated as the ratio between the post processing weight (w), measured using a precision balance, and the geometrical volume (V_{theo}), estimated through the CMM, as reported in Eq. 2:

$$\rho bulk\ [g/cm^3] = \frac{w}{Vtheo}. \quad (2)$$

Porosity evaluation

The deposition process may generate porosity in the internal structure, reducing the bulk density of the samples. The overall porosity (i.e. opened and closed porosity) was estimated to compare the bulk density of the FDM parts printed with different process parameters' combinations to the density of monolithic AISI 316L (ρ_{AISI} = 8 g/cm^3). Specifically, the metal samples were weighed in air (m_1) before being immersed in a wetting liquid (1-butanol, ρ_{fluid}=0.810 g/cm^3) for 24h to fill open porosity. Then, the samples were taken out of the solvent and their surfaces were quickly swabbed before weighing it in air (m_2). The opened porosity (op) and closed porosity fractions (cp) of the sample were calculated, as reported in Eq. 3, Eq.4:

$$op = \frac{m2-m1}{\rho_{fluid}}. \quad (3)$$

$$cp = V_{theo}\ - \frac{m1}{\rho_{AISI}} - \ op. \quad (4)$$

Data analysis

An analysis of variance (ANOVA) was carried out to identify a possible influence of selected process parameters on the final indicators (i.e. apparent density and dimensional shrinkages) and a confidence interval equal to 95% was considered.

Before applying the analysis of variance, a pre-treatment of the data was carried out for identifying possible outlier values by means of the interquartile range (IRQ).

Mechanical test

All metal specimens for the mechanical characterization were printed using the optimal combination of the process parameters resulted from the previous structural analysis. Five samples were printed for each mechanical test.

Tensile test

According to ASTM F3122-14 [9], the procedure outlined in the test method ISO 6892-1:2020 [10] defines the guideline for tension testing under various conditions to determine the material's yield and tensile strengths. These procedures are applicable to components made additively. Tensile tests (5 repetitions) were conducted using a Galdabini testing machine with a 50 kN load cell. The tests were performed orthogonally to the growth direction of the layers, under speed control (0.09 mm/s).

Compressive test

ASTM F3122-14 designates Test Methods E9:2019 [11] as the basic method for uniaxial compression testing of metallic samples, applicable to specimens made additively. Five compression tests were conducted using a BRT hydraulic press with a 1000 kN load cell. The tests were carried out in a parallel direction with respect to the growth of the layers under speed control (0.01 mm/s). Two bearing blocks with a Vickers hardness of 1450 HV were used. A layer of Teflon with a thickness of 0.075 mm was applied to both bearing blocks for minimizing the friction between the elements.

Resilience test

According to ASTM F3122-14, ISO 148-1:2016 [12] includes the guidelines for pendulum impact test for determining the energy absorbed in an impact test of metallic samples produced using additive manufacturing techniques.

Rockwell hardness

ASTM F3122-14 indicates ISO 6508-1:2016 [13] as a standard for the Rockwell hardness (HRB) of additive manufactured parts. The sample was sectioned along the growth direction and a 3x3 line grid was drawn on the internal section. The procedure was repeated for three different samples, obtaining 27 uniformly spaced indentations.

Vickers hardness

The same procedure followed for the Rockwell tests was performed for the Vickers hardness tests, as specified in ISO 6507-1:2018 [14], according to ASTM F3122-14.

Result and Discussion

Density and shrinkage

The outlier analysis identified 3 outliers for the shrinkage along the XY plane; then, they were deleted from the dataset generating an updated version.

Analyzing the p-values obtained by the ANOVA (Table 2), it can be stated that the bulk density is affected by *In*, *s* and *h*. In this case, the T_{nozzle}, as a single parameter, does not affect the results, but it plays an important role in the 2-way interaction. All shrinkage directions show an effect due to the print speed and the layer thickness; while only the Z-Shrinkage is affected by the T_{nozzle}.

As a function of ANOVA results, as demonstrated by the main effect plot (Fig. 1), *In* Line infill, *s* 20 mm/s and *h* 0.1 mm is the combination of process parameters that ensured the highest apparent density of the samples (i.e. 95%). The mentioned optimal process parameters combination generated 16.4% and 20 % shrinkages along XY plan and Z axis, respectively.

Table 2. ANOVA p-values.

	p-value		
	Bulk Density	Planar Shrinkage	Z-Shrinkage
T_{nozzle}	0.0790	0.4920	**0.0000**
In	**0.0030**	0.1900	0.8050
s	**0.0050**	**0.0000**	**0.0010**
h	**0.0000**	**0.0005**	**0.0000**
2-way interaction			
$T_{nozzle} \cdot In$	**0.0060**	**0.1690**	0.0550
$T_{nozzle} \cdot s$	0.1200	0.2550	0.8430
$T_{nozzle} \cdot h$	**0.0030**	**0.0280**	**0.0000**
$In \cdot s$	0.2500	**0.0009**	0.2950
$In \cdot h$	0.3940	0.1400	0.0580
$s \cdot h$	0.0580	0.4440	0.3340

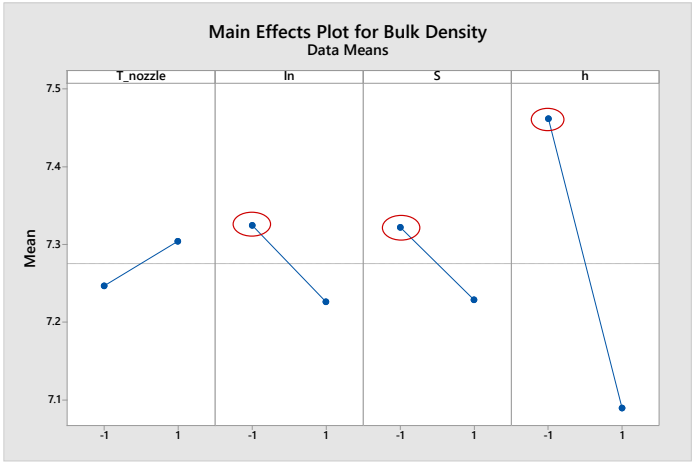

Fig. 1. Main effects plot for bulk density.

Fig. 2a, b and Fig. 3 show the average values and standard deviation for the 4 repetitions of dimensional shrinkages and bulk density , as a function of the printing parameters combination.

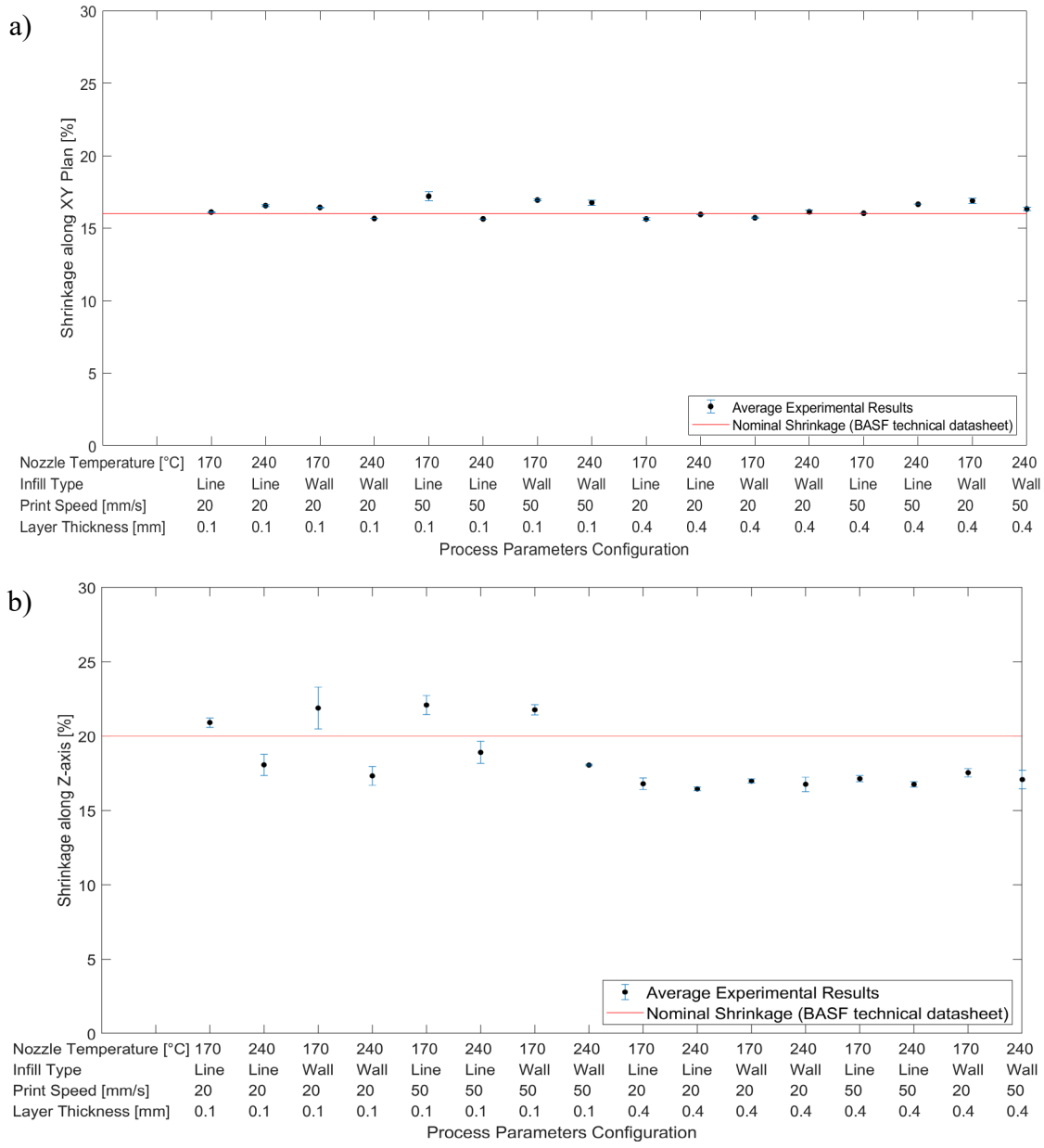

Fig. 2. Average value and standard deviation of shrinkage along XY plan (a) and along Z axis (b) as a function of printing parameters.

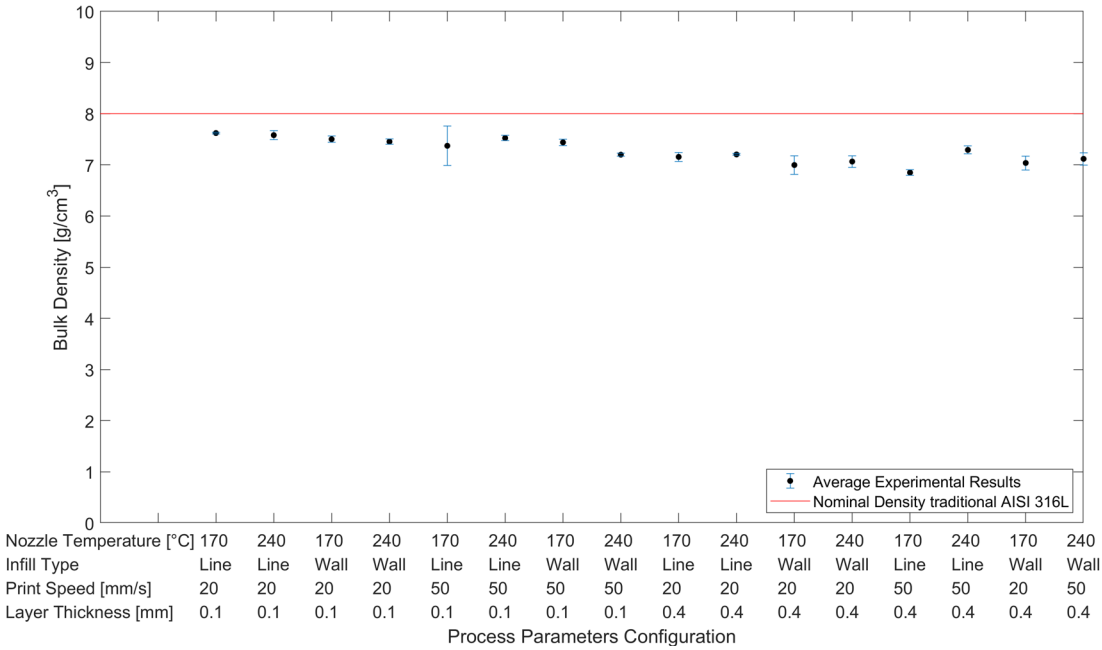

Fig. 3. Average value and standard deviation of bulk density as a function of printing parameters.

Shrinkages calculated on XY plane are close to the nominal value, reported in BASF technical datasheet, showing a good stability of the results. A different distribution can be observed for the shrinkage along Z-axis: the standard deviations are higher and the average values suggest a dissimilar behavior as a function of layer thickness.

Regarding the bulk density of the post-processed parts, in some cases, it appears to be very close to the nominal density of the monolithic AISI 316L, varying in a range between 6.9 and 7.6 g/cm^3.

In all cases, the low standard deviation highlights the stability and repeatability of the process.

The results of the porosity analysis are summarized in Table 3. The samples with the worst bulk density (right column) show a higher percentage of opened porosity due to the poor layer adhesion and the imperfections on the external surfaces. Conversely, the percentage of closed and opened porosity for specimens printed with optimal parameters are lower for T_{nozzle} equal to 170°C (left column).

Table 3. Percentage distribution of effective density, opened (op) and closed (cp) porosities.

	T_{nozzle} 170°C *In* Line *s* 20 mm/s *h* 0.1 mm	T_{nozzle} *240*°C *In* Line *s* 20 mm/s *h* 0.1 mm	T_{nozzle} 170°C *In* Line *s* 50 mm/s *h* 0.4 mm
Effective density	95.3%	94.8%	85.6%
Opened porosity	2.7%	2.5%	12.0%
Closed porosity	2.0%	2.8%	2.4%

Mechanical characterization

The main relevant tensile properties of the tested specimens are summarized in Table 4. The results indicate that the samples printed via FDM technique exhibits poorer mechanical properties than those of the samples made of monolithic AISI 316L.

The average value of yield strength (141.9 ± 14.1 MPa) is lower by 36% compared to that of the monolithic material; the average value of UTS (426.6 ± 23.7 MPa) is lower than that of the monolithic material by approximately 20%. The coarse equiaxed grains generated after the sintering phase could

be a potential issue related to these results [7]. Regarding the elongation at break, the percentage values resulted to be close to those of the monolithic AISI 316L.

Table 4. Tensile properties of 316L FDM samples.

	$\sigma_{f\,02}$ [MPa]	UTS [MPa]	Elongation at break [%]
Sample 1	161.3	464.1	41%
Sample 2	125.0	407.3	37%
Sample 3	134.6	405.9	32%
Sample 4	132.9	409.0	32%
Sample 5	155.7	445.2	38%
AISI 316L	220	530	40%

The tensile test curves, represented in Figure 4, demonstrate the repeatability of the characteristics of printing process. However, the difference in UTS and elongation at break among the samples suggests the possible presence of voids as a result of thermal processes.

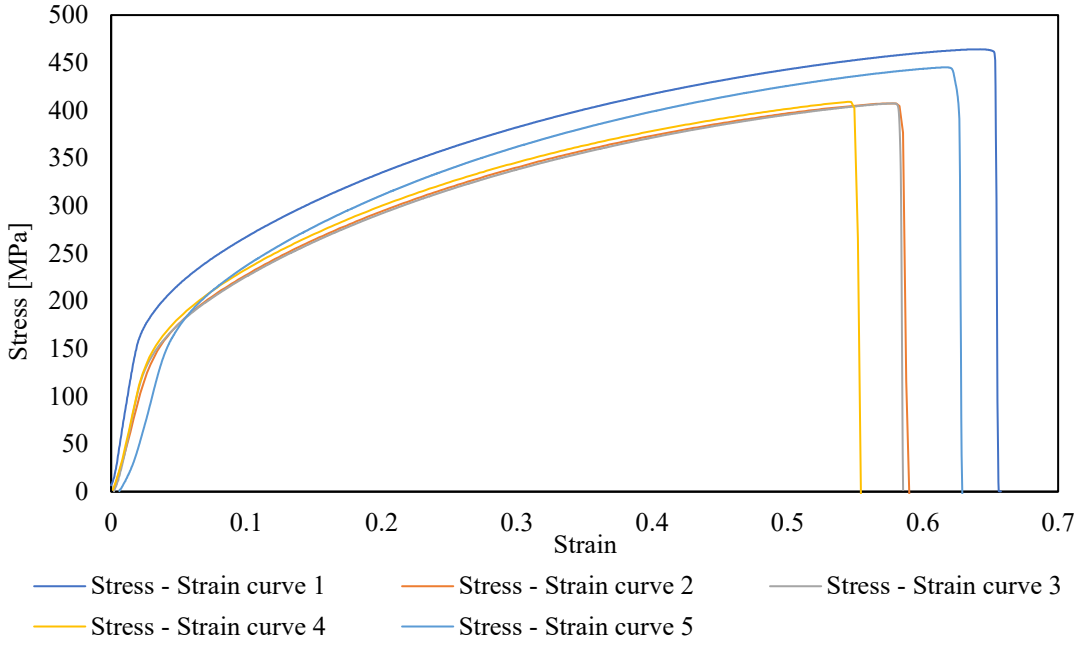

Fig. 4. Tensile stress-strain curves.

The stress–strain graphs of the compression tests are shown in Figure 5. The near–perfect overlap of the compressive curves proves the stability and repeatability of the tests.

Besides, the compression load seems to guarantee an improvement in the compressive stress values of the samples. The average compressive stress of the FDM AISI 316L specimens was 54% lower than that of the tested bulk sample at a strain of 0.1 (dashed line), whereas the average compressive stress value exhibited a deviation of 24% from the value of the bulk specimen at 0.6 strain.

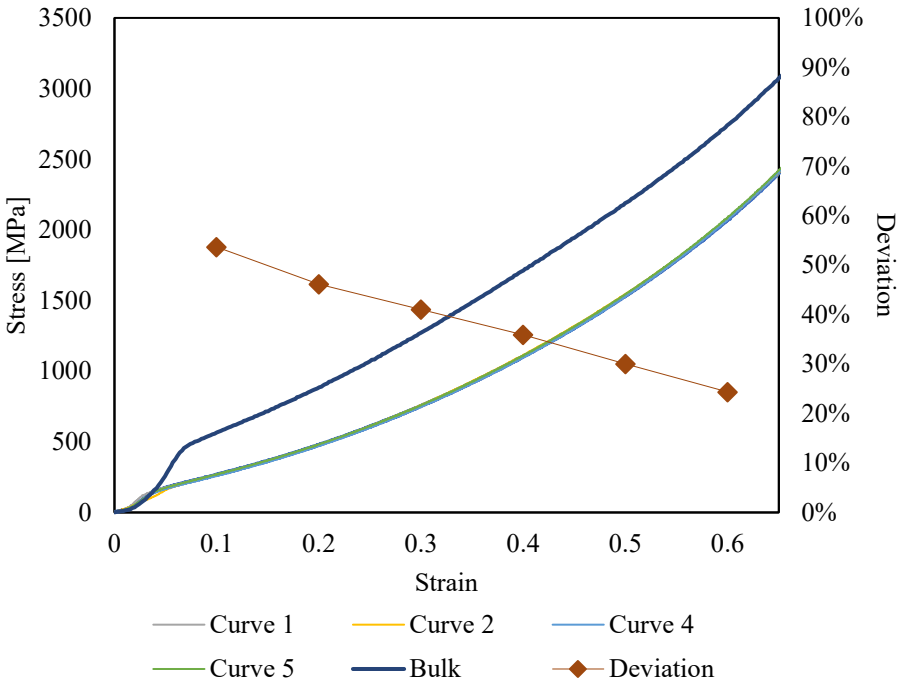

Fig. 5. Compressive stress-strain curves.

The resilience values of the V-notched specimens exhibited an average value of 54.6 ± 8.01 J, which is almost half that of AISI 316L, suggesting brittleness of the metal specimens printed using the Fused Deposition Modeling technology.

The brittleness of the metal FDM samples can be attributed to two main causes. The presence of voids and porosity, as previously reported in Table 3, could reduce the ductility of the samples. Moreover, the X-ray diffraction (XRD) analysis indicates the presence of austenite and δ-ferrite phases (Figure 6). The portion of austenite represents a metallurgical characteristic of the material. On the contrary, the existence of the δ-ferrite phase is merely an effect of the thermal history of the samples which were subjected to an heat treatment during the sintering process. Specifically, the primary δ-ferrite solidifies within the metal matrix and the transformation of δ into γ ferrite may occur during the cooling process of sintering cycle. Since this transformation is a diffusion-controlled process, the fast cooling rate in the sintering cycle (uncontrolled cooling from 1380 °C to room temperature) does not guarantee a sufficiently long time for completing the transformation [15]; thus, portions of δ-ferrite may be retained at the subgrain boundaries of the austenitic matrix of specimens at room temperature [16], with a significant decrease of the strength and ductility and an increment in the stiffness of the parts.

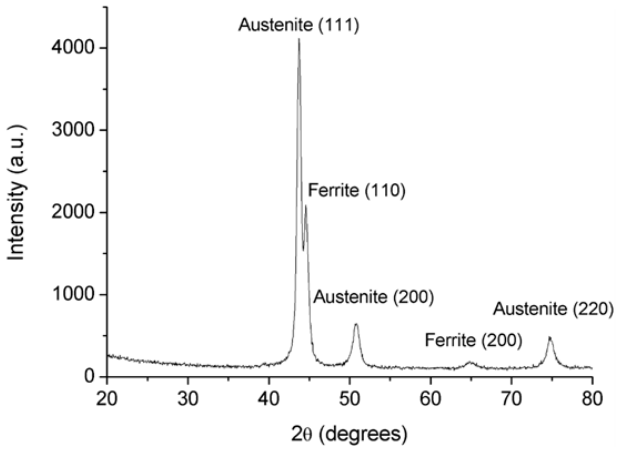

Fig. 6. XRD patterns of the FDM 316L stainless steel

Figure *7* shows Rockwell B and Vickers hardness values depending on their positions on the drawn grid. The average Rockwell B hardness value is approximately 55 ± 4 HRB, which is lower than the monolithic AISI 316L reference value (80 HRB), with a deviation of 32%. Regarding the Vickers hardness, the average value (132.2 ± 3.8 HV) is approximately 15% lower with respect to the value of the monolithic AISI 316L (155 HV).

Furthermore, the uniform distribution of both hardness values along the growth direction of the layers may suggest the isotropic behaviour of the material.

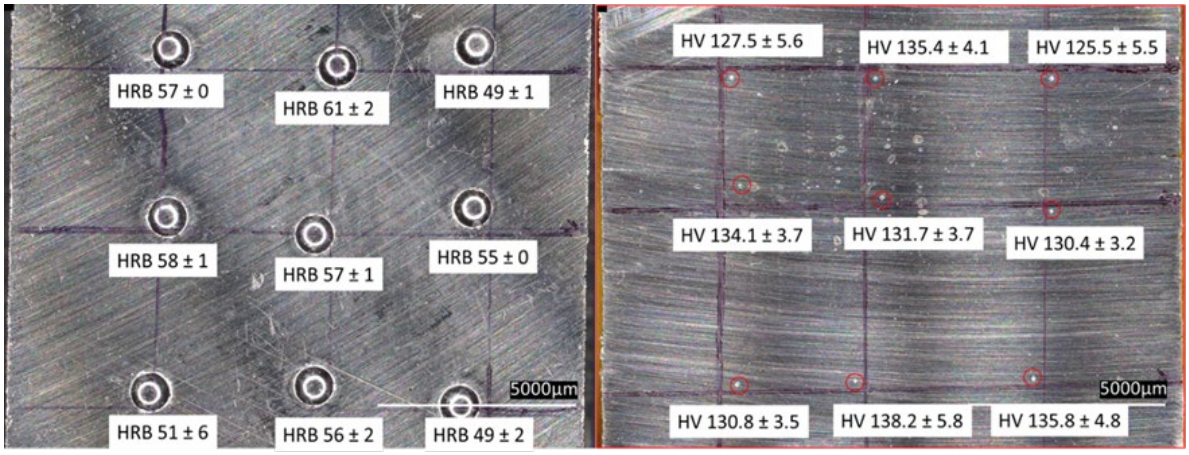

Fig. 7. Rockwell B Hardness (left) and Vickers hardness (right) values in their relative positions within the sample.

Conclusion

This study discusses the application of a metal filament on a FDM machine to print metal parts with good mechanical properties. This innovative solution may overcome time and cost limits connected with the traditional metal Additive Manufacturing technologies. The first part of the study is focused on the determination of the optimal combination of printing parameters, testing several conditions and defining the combination that allows to obtain a density as close as possible to the nominal value of the monolithic material. In the second part, the mechanical characteristics of samples printed using the optimized parameters were evaluated following the international standard ASTM F3122-14.

Considering the structural analysis, it is evident that both bulk density and dimensional shrinkages along all directions are affected by the process parameters. Shrinkage along XY plane (about 16.40%) exhibited a good stability around the nominal shrinkage. On the contrary, the interaction between the nozzle temperature and other process parameters generated higher variability along Z axis. The optimized combination *In* Line, *s* 20 mm/min and *h* 0.1 mm ensured the realization of metal samples with a 95% of relative density.

The conducted mechanical characterization indicated that tensile specimens printed via FDM technique exhibited lower values of yield strength and UTS compared to those of the monolithic material. The compression action on the specimens enhanced the average stress value in direct proportion to the increase in strain. Both Rockwell B and Vickers hardness tests verified the isotropic behavior of the samples along the growth direction. An XRD analysis showed the abnormal presence of δ-ferrite in the austenitic matrix, which may explain the brittleness of the FDM metal specimens.

Based on the results obtained through the performed tests, metal Fused Deposition Modelling can be considered as a promising cost-effective approach for the fabrication of metal components for different industrial applications.

References

[1] ISO/ASTM 52900:2017, ASTM Int. (2017).

[2] S. Hwang, E.I. Reyes, K. sik Moon, R.C. Rumpf, N.S. Kim, Thermo-mechanical Characterization of Metal/Polymer Composite Filaments and Printing Parameter Study for Fused Deposition Modeling in the 3D Printing Process, J. Electron. Mater. 44 (2015) 771–777.

[3] M.A. Ryder, D.A. Lados, G.S. Iannacchione, A.M. Peterson, Fabrication and properties of novel polymer-metal composites using fused deposition modeling, Compos. Sci. Technol. 158 (2018) 43–50.

[4] J. Gonzalez-Gutierrez, D. Godec, C. Kukla, T. Schlauf, C. Burkhardt, C. Holzer, Shaping , Debinding and Sintering of Steel Components Via Fused Filament Fabrication, 16th Int. Sci. Conf. Prod. Eng. - CIM2017. (2017).

[5] J. Gonzalez-Gutierrez, S. Cano, S. Schuschnigg, C. Kukla, J. Sapkota, C. Holzer, Additive manufacturing of metallic and ceramic components by the material extrusion of highly-filled polymers: A review and future perspectives, Materials (Basel). 11 (2018).

[6] B. Liu, Y. Wang, Z. Lin, T. Zhang, Creating metal parts by Fused Deposition Modeling and Sintering, Mater. Lett. 263 (2020) 127252.

[7] T. Kurose, Y. Abe, M.V.A. Santos, Y. Kanaya, A. Ishigami, S. Tanaka, H. Ito, Influence of the Layer Directions on the Properties of 316L Stainless Steel Parts Fabricated through Fused Deposition of Metals, (2020).

[8] H. Gong, D. Snelling, K. Kardel, A. Carrano, Comparison of Stainless Steel 316L Parts Made by FDM- and SLM-Based Additive Manufacturing Processes, Jom. 71 (2019) 880–885.

[9] ASTM F3122-14, ASTM Int. 10.04 (2014) 6.

[10] ISO 6892-1:2020, Int. Stand. (2020).

[11] ASTM E9:2019 - Standard Test Methods of Compression Testing of Metallic Materials at Room Temperature, ASTM Int. 03.01 (2019).

[12] ISO 148 - 1:2016 - Metallic materials - Charpy pendulum impact test, Int. Stand. (2016).

[13] ISO 6508-1:2016 - Metallic materials - Rockwell hardness test Test method, Int. Stand. (2016).

[14] ISO 6507-1:2018 - Metallic materials - Vickers hardness test Test method, Int. Stand. (2018).

[15] M. Dadfar, M.H. Fathi, F. Karimzadeh, M.R. Dadfar, A. Saatchi, Effect of TIG welding on corrosion behavior of 316L stainless steel, Mater. Lett. 61 (2007) 2343–2346.

[16] M. Ziętala, T. Durejko, M. Polański, I. Kunce, T. Płociński, W. Zieliński, M. Łazińska, W. Stępniowski, T. Czujko, K.J. Kurzydłowski, Z. Bojar, The microstructure, mechanical properties and corrosion resistance of 316 L stainless steel fabricated using laser engineered net shaping, Mater. Sci. Eng. A. 677 (2016) 1–10.